Journal of Medicinal Chemistry

Article

Dynamic Generation of G-quadruplex DNA Ligands by Target-Guided Combinatorial Chemistry on a Magnetic Nano-platform

Snehasish Jana, Deepanjan Panda, Puja Saha, Dan Pantos, and Jyotirmayee Dash

J. Med. Chem., **Just Accepted Manuscript** • DOI: 10.1021/acs.jmedchem.8b01459 • Publication Date (Web): 11 Dec 2018

Just Accepted

ACS Publications

is published by the American Chemical Society. 1155 Sixteenth Street N.W., Washington, DC 20036

Dynamic Generation of G-quadruplex DNA Ligands by Target-Guided Combinatorial Chemistry on a Magnetic Nano-platform

*Snehasish Jana[†][a], Deepanjan Panda[†][a], Puja Saha[a], G. Dan Pantoș[b] and Jyotirmayee Dash[a]**

[a] School of Chemical Sciences, Indian Association for the Cultivation of Science, Jadavpur, Kolkata-700032, India, E-mail: ocjd@iacs.res.in; Fax:+91-33-2473-2805; Tel: +91-33-2473-4971, ext 1405.

[b] Department of Chemistry, University of Bath, Claverton Down, Bath, BA2 7AY (UK)

ABSTRACT: Dynamic combinatorial chemistry (DCC) has emerged as a promising strategy for template-driven selection of high-affinity ligands for biological targets from equilibrating combinatorial libraries. However, only a few examples using disulphide exchange based DCC are reported for nucleic acid targets. Herein, we have demonstrated that gold-coated magnetic nanoparticle conjugated DNA targets can be used as templates for dynamic selection of ligands from an imine-based combinatorial library. The implementation of dynamic combinatorial chemistry using DNA-nanotemplates enables efficient identification of the lead compounds, from the DCL via magnetic decantation. It further allows quick separation of DNA-nanotemplates for reuse in DCC reactions. The identified lead compound exhibits significant

quadruplex-vs.-duplex DNA selectivity and suppresses promoter activity of *c-MYC* gene that contains G-quadruplex DNA forming sequence in the upstream promoter region. Further cellular experiments indicated that the lead compound is able to permeate into cell nuclei and trigger a DNA-damage response in cancer cells.

INTRODUCTION

Target-guided synthetic (TGS) approaches have been considered as powerful strategies to discover novel and selective small molecules for biological targets by bridging the gap between chemical synthesis and screening assays.[1-8] Dynamic Combinatorial Chemistry (DCC), a thermodynamically controlled target-guided synthetic approach has been employed for the identification of selective ligands in a cost- and time-effective manner.[1-8] In DCC, simple molecular building blocks assemble through reversible bond formation to generate a dynamic combinatorial library (DCL) consisting of a mixture of continuously inter-convertible products. In the presence of a template, the equilibrium of the system shifts towards the formation of those DCL components that strongly bind to the template at the expense of weak binders. Thus, this concept provides an unique platform for the in-situ generation of high-affinity binders, offering new opportunities for bio-medicinal applications.[9-14] DCC has also been effectively used for the development of hosts for small molecules,[10] interlocked molecules,[11,12] and catalysts[13] as well as for the functionalization of liposomes, nanoparticles etc.[14]

However, only a limited number of studies have been reported for the development of small molecule probes for proteins[15-18] and nucleic acids.[19-27] The Miller group first reported the application of DCC to generate ligands for double stranded DNA.[19] The Balasubramanian group used disulphide chemistry based DCC to identify selective binders for G-quadruplex targets.[22-24] DCC has also been used for developing RNA binding ligands.[25-27] To improve the identification

of small molecule ligand(s) from DCL, Miller and co-workers have devised resin bound DCC[28] and the Otto group has recently reported nanoparticle functionalized building blocks for DCC.[29-30] Most of these studies employ the disulphide-exchange chemistry that has several advantages like water compatibility and very fast thiol-exchange property at mild pH.[31] However, the resulting disulphide leads may lose their druggability due to their instability in cellular environment.[32] On the other hand, imine-exchange based DCC using aldehyde and amine building blocks produces the imine-leads, which could be reduced to stable amine products[15, 20] for further biophysical and cellular studies.

In this study, we have employed gold-coated magnetic nanoparticle-conjugated G-quadruplex DNA (G_4-DNA nano-template), as templates[33] for dynamic selection of G-quadruplex DNA ligands from aldehyde and amine building blocks. We envisaged that the G_4-DNA nano-template would accelerate the identification of high-affinity ligands by providing multiple templates on the surface of gold coated magnetic nanoparticles, simplify the separation of ligands and enable the isolation of DNA nano-template by magnetic decantation. The selective ligands have the potential to exhibit anticancer activities by stabilizing the quadruplex nucleic acids.[34-43]

RESULTS AND DISCUSSION

Design and synthesis of aldehyde and amine building blocks. In our design, we have used a carbazole aldehyde **1** and a series of amines **2a-j** (**Scheme 1**) to develop specific ligand for G-quadruplex DNA. Carbazole aldehyde **1** was selected as a building block as it can interact with the terminal quartets of G_4-DNA via π–π aromatic stacking interactions.[33,44] The aldehyde **1** was prepared from commercially available carbazole via mono-iodination, N-alkylation followed by Vilsmeier-Haack formylation[45] and Suzuki coupling[46] in good overall yield (**Figure S1**,

Supporting Information, S.I.). The 10-membered amine library **2a-j** includes aromatic and aliphatic amines that could be involved in electrostatic and hydrogen bonding interactions with DNA structures. The amines possess comparable reactivity to avoid biasness in the competition.

Scheme 1. (a) Aldehyde (1) and amine (2a-j) building blocks for DCC (b,c) 10 member dynamic combinatorial imine (3a-j) library and the corresponding reduced imines (4a-j).

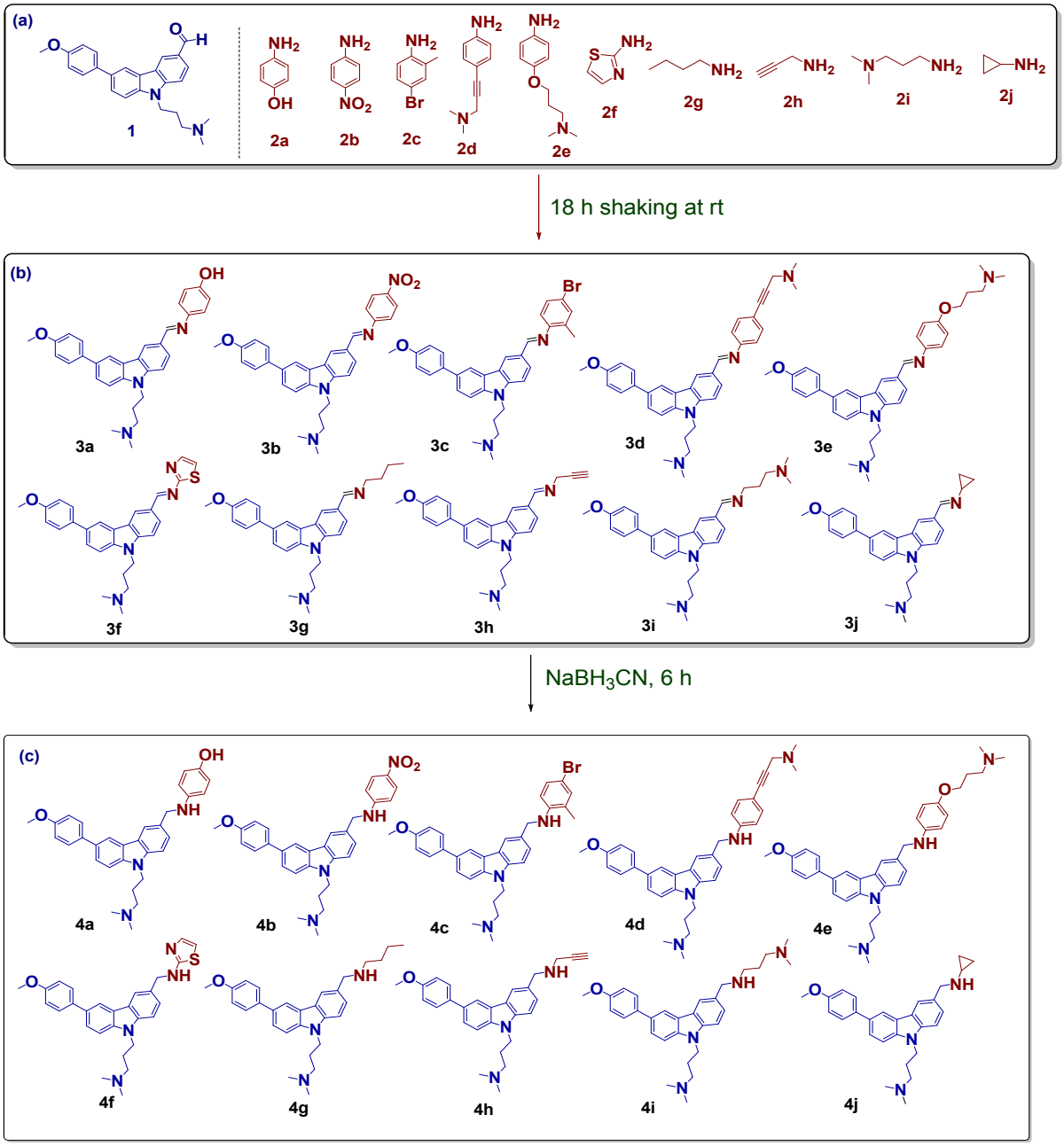

The aldehyde **1** and amines **2a-j** building blocks would reversibly react to form imines **3a-j** under near physiological conditions. Subsequently, the imine(s) formed could be irreversibly reduced to stable amines **4a-j** by $NaBH_3CN$ providing an equilibrated mixture for analysis. The reversibility of the reaction is a key factor for developing a Dynamic Combinatorial Library (DCL). To establish the reversibility of the system, aldehyde **1** was continuously stirred with an excess of amine **2e** in MOPS buffer (20 mM, pH 6.5) containing 100 mM KCl for 12 h. The MOPS buffer was used to maintain a slightly acidic medium, which is optimal for imine exchange reaction and the buffer system containing 100 mM KCl is suitable to maintain the four stranded conformation of the G_4-DNA in near physiological pH.[47] An aliquot of the resulting mixture was analyzed by ESI mass spectrometry confirming the formation of the corresponding imine **3e** (**Figure S2**). The amine **2d** was then added in excess to the reaction mixture and the reaction was continued for another 12 h. The ESI mass analysis of the resultant mixture showed the presence of both the imines **3d** and **3e** (**Figure S3**). The formation of both imines indicates that imine **3e** was converted to imine **3d** via reversible exchange and thus, these building blocks are suitable for DCC reaction (**Scheme 2**).

Scheme 2. Reversible exchange between imines 3e and 3d in MOPS buffer (20 mM, pH 6.5) containing 100 mM KCl.

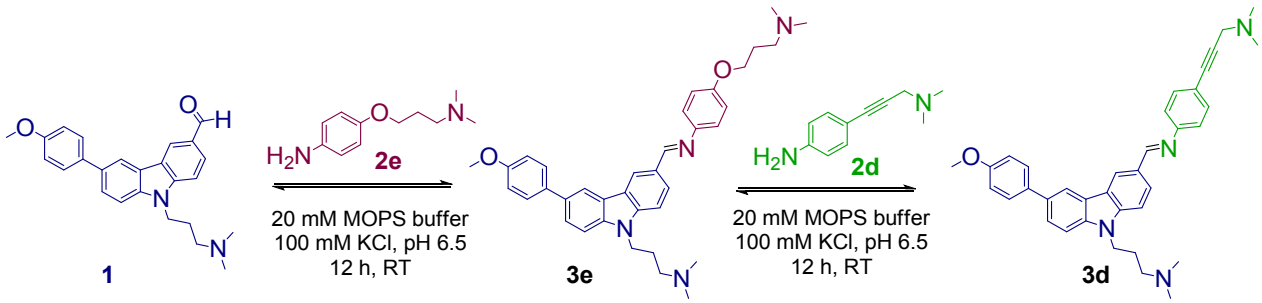

DNA templated imine exchange DCC. The 10-membered amine library (**2a**-**2j**) was then exposed with the aldehyde **1** to form a DCL and left to equilibrate for 18 h at 25 °C in MOPS buffer (20 mM, pH 6.5) with 100 mM KCl. Five-fold excess of each amine was used for the complete consumption of aldehyde **1**. Then, $NaBH_3CN$ was added to the reaction mixture and incubated for 6 h at the same temperature for switching the system towards irreversibility. The HPLC chromatogram of this reaction mixture provided overlapping peaks and ESI mass analysis of the HPLC fractions revealed the formation of all the corresponding amines **4a**-**j** without any considerable selection (**Figure 3a**).

The reaction was then performed in the presence of a G-quadruplex nano-template (G_4-AuMNp) and a duplex DNA nano-template (*ds*DNA-AuMNp) under similar reaction conditions. We have taken a thiolated G-quadruplex forming sequence present in the promoter region of *c-MYC* oncogene.[48,49] The G_4-AuMNp was prepared by immobilizing thiolated G_4-DNA on gold-coated magnetic nanoparticles. Similarly, a control self-complementary duplex DNA nanotemplate, (*ds*DNA-AuMNp) was prepared by attaching a thiolated *ds*DNA sequence on gold-coated magnetic nanoparticles (**Figure 1a**). The G_4-AuMNp and *ds*DNA-AuMNp templates were characterized by using TEM, UV-Vis and Circular Dichroism spectroscopy. These studies revealed that DNA functionalized nanoparticles were 10-15 nm in diameter (**Figure 1b** & **1d**) and they displayed absorption peaks near 260 nm along with the typical SPR peak of Au at 535 nm (**Figure 1e-f**). The G_4-AuMNp exhibited a positive peak at 260 nm and negative peak at 240 nm in CD spectroscopy indicating that G_4-AuMNp maintains the parallel conformation of G-quadruplex structure (**Figure 1c**). The CD spectrum of *ds*DNA-AuMNp also showed a positive signal at 275 nm and a negative signal at ~250 nm corresponding to the duplex DNA

conformation (**Figure 1c**). Moreover, these DNA coated magnetic nanoparticles could be easily dispersed in aqueous media and could also be isolated by using magnetic separation.

In order to perform DCC reactions with DNA nano-templates, the aldehyde and amine building blocks were incubated in the presence of G_4-AuMNp or *ds*DNA-AuMNp for 18 h in MOPS buffer (20 mM, 100 mM KCl), pH 6.5 at RT. To this mixture of interconvertible imines, $NaBH_3CN$ was added and the mixture was stirred for 6 h for the complete reduction of imines to the corresponding amines; thus, the system became irreversible (**Figure 2**, **Figure S4**). Subsequently, amine bound DNA nano-templates were separated by magnetic decantation and the unbound amines remained in the supernatant. The isolated DNA-AuMNps were washed three times with MOPS buffer and the resulting suspension was heated at 65 °C to release the template bound amine products. Then DNA-AuMNps were instantly separated by an external magnet and the supernatant was characterized by HPLC and ESI-MS analysis to identify the lead amine products.

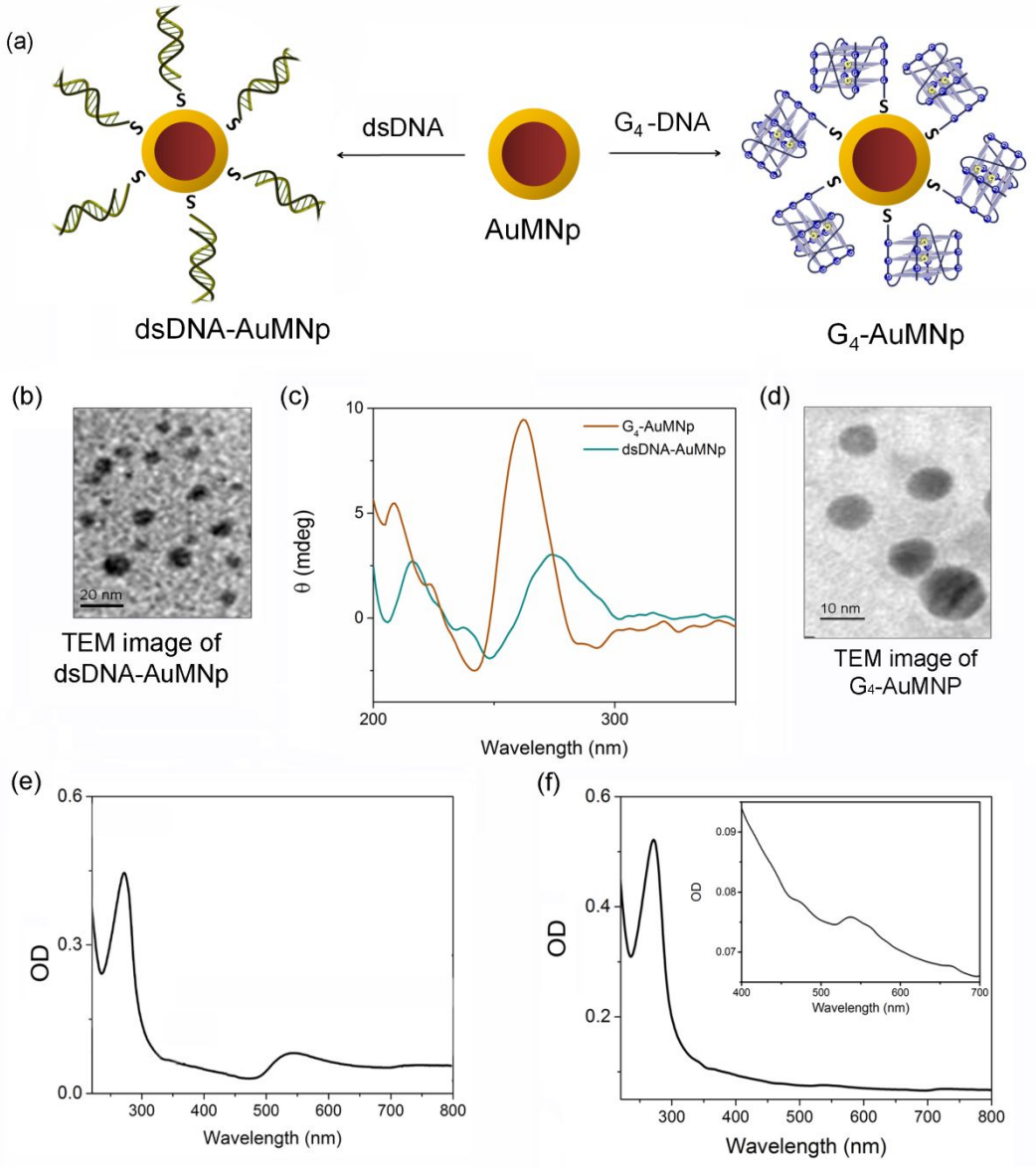

Figure 1. (a) Schematic representation of the preparation of G_4-AuMNp (Seq.: 5'-[ThiC6]-$TG_4AG_3TG_4AG_3TG_4A_2G_2$-3') and *ds*DNA-AuMNp (Seq.: 5'-[ThiC6]-$CA_5T_5GCA_5T_5G$-3'). (b) TEM image of *ds*DNA-AuMNp. (c) CD spectra of G_4-AuMNp and *ds*DNA-AuMNp in 20 mM MOPS buffer (pH 6.5, 100 mM KCl). (d) TEM image of G_4-AuMNp. (e-f) Absorption spectra of *ds*DNA-AuMNp and G_4-AuMNp in 20 mM MOPS buffer (pH 6.5, 100 mM KCl).

Significant changes in the composition of DCL were observed in the presence of G_4-DNA and *ds*DNA nano-templates (G_4-AuMNp and *ds*DNA-AuMNp) (**Figure 3** and **Figure S5**). The HPLC retention times and the mass analysis of the products revealed that amine **4e** (reduced product of imine **3e**, derived from **1** and **2e**) was exclusively obtained in the presence of G-quadruplex nano-template out of 10 possible amine products **4** (**Figure 3f**). In the presence of *ds*DNA nano-template, five amine products **4g**, **4h**, **4i**, **4f** and **4b** (reduced products of imines **3g**, **3h**, **3i**, **3f** and **3b**, respectively) were identified (**Figure 3b**). These results indicate that amine **4e** is a selective lead for the G-quadruplex target. Furthermore, **4e** was exclusively obtained by giving a shorter reaction time (i.e. 30 min to 4 h) for the reduction step (**Figure S6**, **S.I.**).

Next, we performed the DCC using the same aldehyde and amine library and after 18 h equilibration period, the imine-bound G_4-AuMNps were separated and reduced by $NaBH_3CN$. The HPLC and ESI-MS results revealed that ligand **4e** was exclusively obtained, indicating G_4-AuMNp selects the best binder (i.e. **3e**) from the imine DCL due to higher affinity of imine **3e** and then **3e** was reduced to stable amine (**4e**) upon addition of $NaBH_3CN$ (**Figure S7**, **S.I.**). In comparison, by using solution phase DCC with free quadruplex DNA, we observed a complex mixture of compounds in the HPLC chromatogram (**Figure S8**), making lead identification difficult.

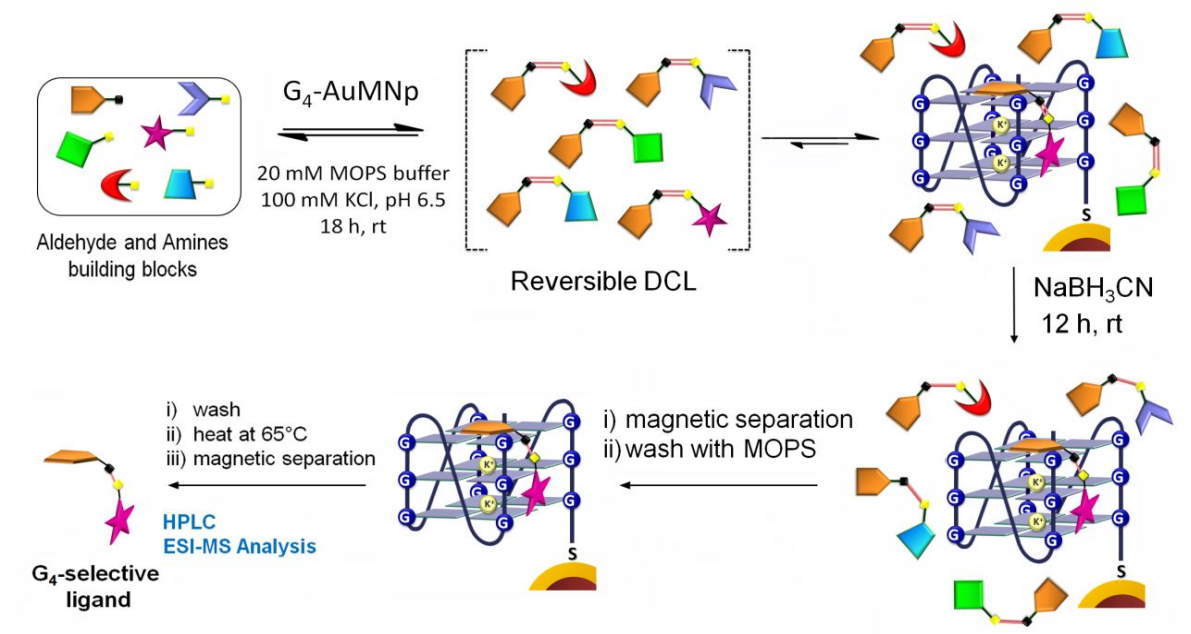

Figure 2. Schematic representation of imine exchange based dynamic combinatorial chemistry using G_4-AuMNp template.

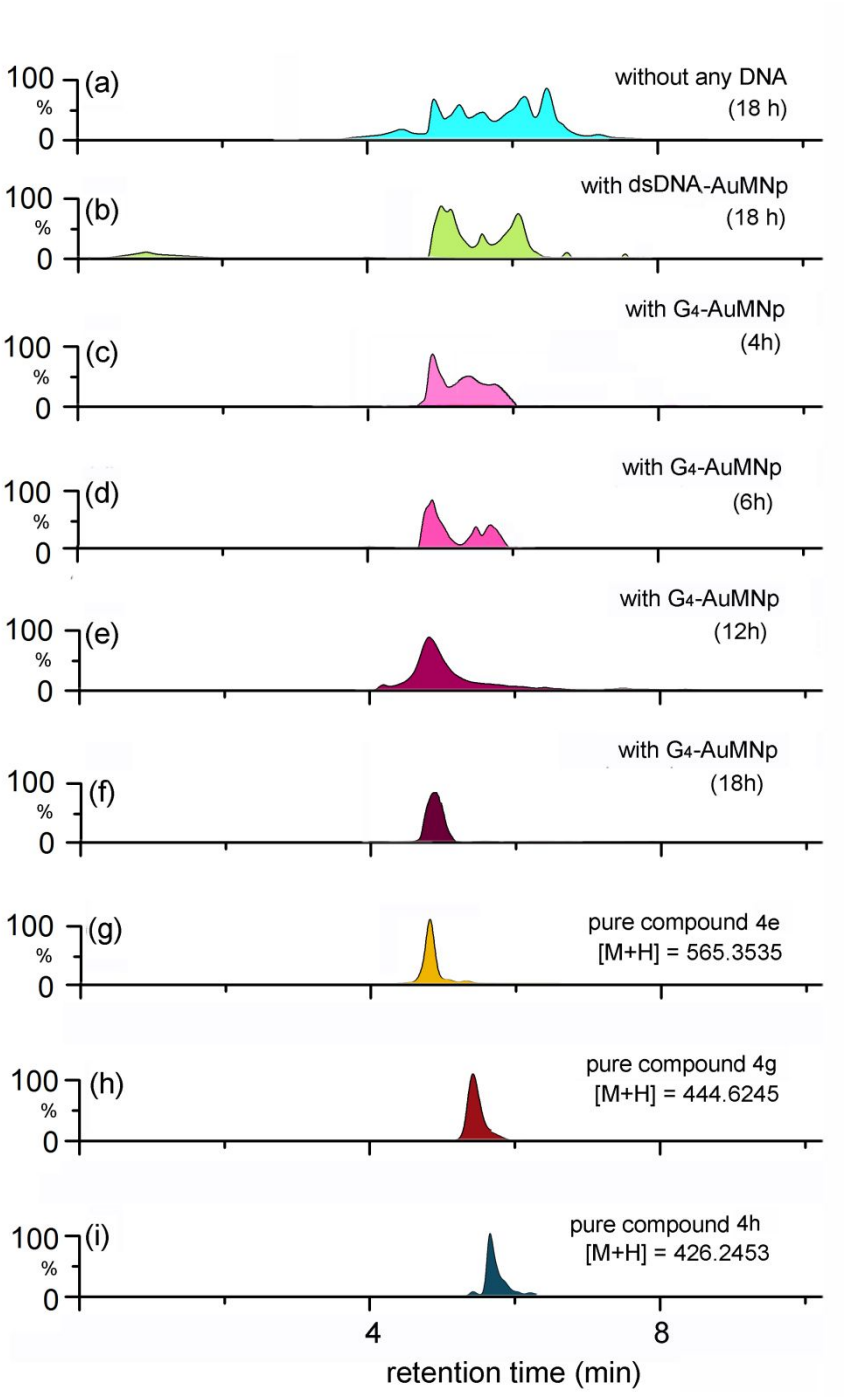

Figure 3. HPLC analysis of the DCL (a) without any external template and using (b) *ds*DNA-AuMNp and (c-f) G_4-AuMNp after 4 h, 6 h, 12 h, 18 h respectively. HPLC chromatogram of pure compound (g) 4e (h) 4g and (i) 4h.

Next, we carried out a time-dependent imine exchange DCC reaction of the same library in the presence of G_4-AuMNp to optimize the time required for the amplification of **4e**. For this purpose, we collected aliquots of the reaction mixture after 4 h, 6 h, 12 h and 18 h and then reduced using $NaBH_3CN$. Following the similar procedure, the lead compounds were isolated from each reaction mixture using magnetic separation and then analyzed by HPLC and ESI-MS (**Figure 3c-e**). The time-dependent HPLC analysis revealed that ligands **4e**, **4g** and **4h** were formed in a ratio of ~ 25:12:10 respectively after 4 h, indicating the corresponding imines **3e**, **3g** and **3h** were in equilibrium in the presence of G_4-DNA nanotemplates. As the time progressed, continuous elevation in the LC response signal of **4e** was noticed and the LC response signals of **4g** and **4h** were gradually decreased at 6 and 12 h time period. Finally, after 18 h, ligand **4e** was exclusively formed and by giving longer equilibration time up to 48 h, ligand **4e** was obtained as the sole product (**Figure S9**, **SI**), illustrating that the system has reached thermodynamic equilibrium by 18 h. For further validation, the DCL was pre-equilibriated for 24 h and then incubated with G_4-AuMNp for 18 h; this DCL also produced **4e** exclusively. These observations indicate that among the possible amine products, **4e** exhibits higher binding affinity and selectivity for the G_4-DNA over dsDNA (**Figure 4**) as other lead products **4g** and **4h** were also formed in the presence of dsDNA nanotemplate. Furthermore, when we mixed the G_4-AuMNp with all the synthesized amines (pure **4a-j**), LC response of **4e** and **4g** was observed (**Figure S10**, **S.I.**), indicating that the amplification of **4e** in DCC is not mediated by mere affinity capture by DNA templates. Here, the imine DCL evolves and self-corrects in the presence of G_4-nanotemplate to amplify its best binder at the expense of other weak imine products. It is also interesting to mention that the quadruplex nano-template could be recovered and reused for five DCC reaction cycles (**Figure S11, S12**, **S.I.**).

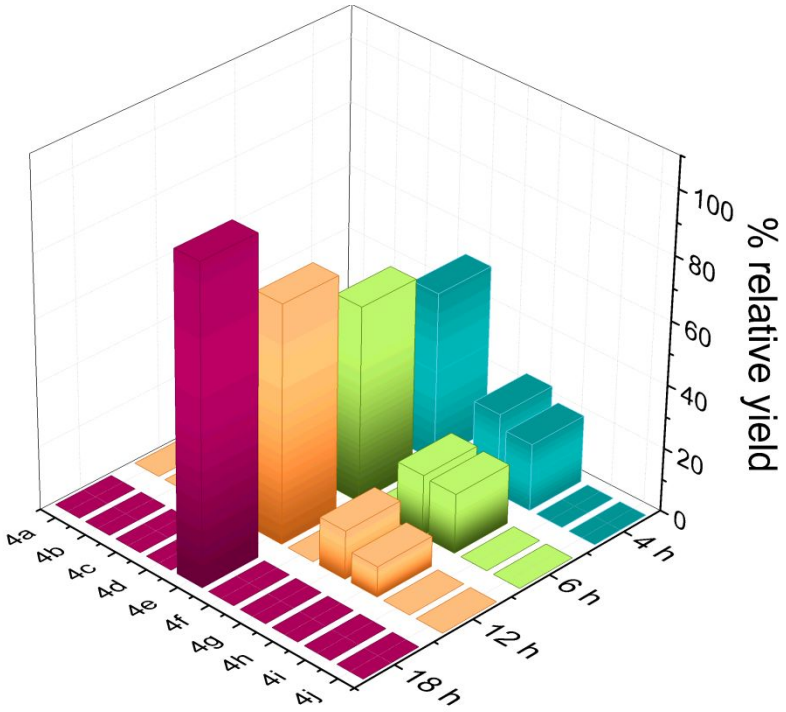

Figure 4. Comparison of relative composition of the DCL in presence of G_4-AuMNp with time interval of 4 h, 6 h, 12 h and 18h.

Validation of lead compounds by biophysical analysis. To further validate these findings, all possible amine products (**4a-4j**) were synthesized (**Figure S13**, **S.I.**) and their ability to stabilize the G-quadruplex DNA was investigated by Förster Resonance Energy Transfer (FRET) based DNA melting assays[50] using FAM and TAMRA labelled G-quadruplex and double stranded DNA sequences at 1 μM ligand concentration (**Table 1**, **Figure S14**, **S.I.**). Interestingly, the lead compound **4e** showed high stabilization potential for G_4-DNA (ΔT_m = 23.4 °C) over dsDNA (ΔT_m = 0.6 °C). The other two lead two compounds **4g** and **4h** showed ΔT_m values of 13.6 °C and 11.8 °C for G_4-DNA and ΔT_m values of 9.5 °C and 8.5 °C for dsDNA, respectively. Ligands **4a** with aromatic hydroxyl group, **4b** with aromatic nitro group, bromo-substituted amine product **4c** and **4d** with tertiary propyl amine side chain, **4f** with thiazole side chain and **4j** with neutral cyclopropane side chain exhibited weak stabilization potentials with low ΔT_m values for G_4 and duplex DNA. The cationic tertiary amine side chain containing compound **4i** showed

moderate stabilization potential for both dsDNA (ΔT_m = 7.2 °C) and G_4-DNA (ΔT_m = 5.3 °C). In addition, to assess the selectivity of ligand **4e** for G_4-DNA, we performed competitive FRET experiments with 0.2 μM of labelled G_4-DNA (*c-MYC*) and 1 μM **4e** with increasing concentrations of non-labelled calf-thymus duplex DNA (ctDNA) competitor. These results showed that the ΔT_m value of *c-MYC* G_4-DNA with 1 μM **4e** was not altered in the presence of excess ctDNA (1-200 eq of *c-MYC* G_4-DNA) (**Figure S15, S.I.**), indicating ligand's selectivity for quadruplex DNA over duplex DNA. Circular Dichroism spectroscopy further revealed that the characteristic CD signature for the native parallel topology of *c-MYC* G_4-DNA (a positive peak at 260 nm and a negative peak at 240 nm) was retained in the presence of ligand **4e**, even at 10 eq concentrations (**Figure S16, S.I.**). These suggest that **4e** binds and stabilizes the quadruplex DNA without perturbing its parallel conformation.

Table 1. ΔT_m values of ligands at 1 μM concentration for *c-MYC* G_4 and *ds*DNA in 60 mM potassium cacodylate buffer, pH 7.4.

Ligands	ΔT_m (°C)	
	c-MYC G_4	*ds*DNA
4a	0.7	1.9
4b	3.4	2.4
4c	3.3	0.44
4d	5.0	3.79
4e	23.4	0.58
4f	3.2	1.15
4g	13.6	9.5
4h	11.8	8.5
4i	5.3	7.2
4j	3.5	1.1

T_m of *c-MYC* G_4-DNA is 70.1°C and *ds*DNA is 65°C in the absence of ligands. DNA concentration: 200 nM.

The binding affinities of the lead compounds (**4e**, **4g** and **4h**) for G_4-DNA and *ds*DNA were determined using fluorescence spectroscopic titrations. As shown in **Figure 5**, ligand **4e** exhibited emission maximum at 400 nm (λ_{max}^{em}) when excited at 300 nm (λ_{ex}). Upon incremental addition of G_4-DNA, the emission intensity of **4e** at 400 nm was enhanced by 4.4 fold and a large red-shift of 50 nm of the emission maximum was observed eventually leading to a new emission maximum at around 450 nm (**Figure 5a, Figure S17, SI**). The observed red shift arises from the strong binding interactions of **4e** with DNA G-quadruplex, which restricts the rotation of the 4-methoxy phenyl ring relative to the carbazole moiety in the excited state. With *ds*DNA, no significant change in the fluorescence intensity of **4e** was observed indicating its excellent selectivity for G-quadruplex DNA (**Figure 5b**). The titration of compound **4g** (λ_{max}^{em} = 397 nm, λ_{ex} = 300 nm) with G_4-DNA and *ds*DNA showed that the fluorescence intensity was decreased by 2.3-fold and 1.5 fold respectively (**Figure 5c-d**). The fluorescence intensity of **4h** (λ_{max}^{em} = 396 nm, λ_{ex} = 300 nm) was also decreased by 1.5 fold with both G_4-DNA and *ds*DNA (**Figure 5e-f**). Ligand **4e** displayed an apparent K_d value of 1.08 ± 0.2 μM for G_4-DNA whereas **4g** and **4h** showed higher K_d values for G_4-DNA (**Table 2**). These results are consistent with the results obtained using DCC, suggesting that ligand **4e**, exclusively formed in the presence of G_4-AuMNp shows selective binding affinity to G_4-DNA compared to other lead compounds **4g** and **4h** formed by giving short equilibration time (4-12 h).

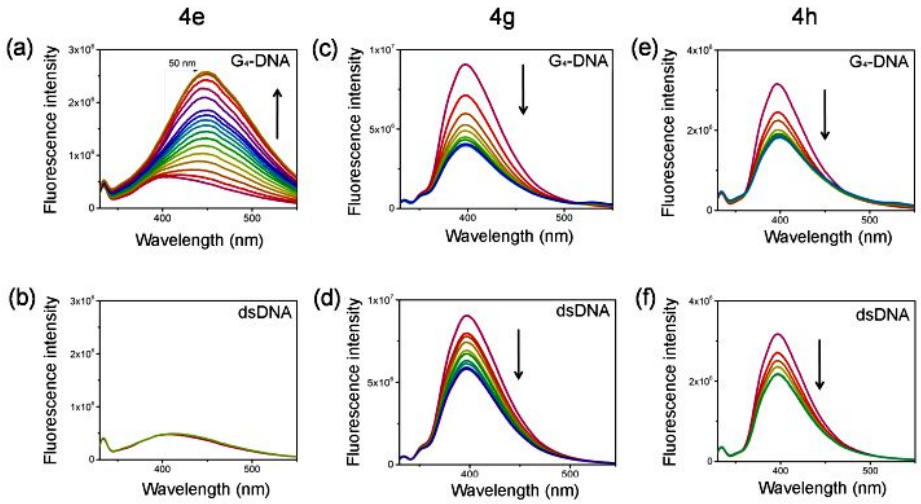

Figure 5. Fluorescence emission spectra of lead compounds with G_4-DNA and *ds*DNA. Conditions: [Ligand] = 0.25 µM; 100 mM Tris.KCl buffer, pH 7.4, Excitation wavelength 300 nm.

Table 2. Apparent dissociation constants (K_d) obtained from fluorimetric titration and DC_{50} values obtained from FID assay for the lead compounds for G_4-DNA and *ds*DNA in 100 mM Tris.KCl buffer (pH 7.4).

Ligands	K_d (µM)		DC_{50} (µM)	
	G_4-DNA	*ds*DNA	G_4-DNA	*ds*DNA
4e	1.08 ± 0.2	N.d.	2.25	> 30
4g	5.72 ± 0.1	6.63 ± 0.3	8.01	> 30
4h	7.17 ± 0.3	7.03 ± 0.2	> 25.0	> 30

The binding selectivity of the lead compounds for G-quadruplex DNA over duplex DNA was further corroborated by using Fluorescence intercalator displacement assay[51] (FID, **Figure S18**). The FID assay was carried out using Thiazole orange (TO) as the fluorescent intercalator. For each ligand, FID experiments were performed with both G_4-DNA and *ds*DNA and the binding

affinities of ligands were evaluated in terms of DC_{50} values. In agreement with Fluorescence binding titrations, ligand **4e** exhibited a significantly higher ability to displace 50% TO from G_4-DNA (DC_{50} = 2.25 μM) compared to *ds*DNA (DC_{50} > 30 μM) (**Figure S18**). The DC_{50} value of **4g** was determined to be 8.0 μM for the G_4-DNA and > 30 μM for *ds*DNA. In comparison, the 50 % threshold limit was not acquired by **4h** for the G_4-DNA and *ds*DNA even at a concentration of 25 μM (DC_{50} > 25 μM) (**Table 2**). The FRET melting assay, fluorescence binding titrations and FID studies establish a direct correlation between DNA-mediated amplification of selective leads and their binding affinities for the DNA targets.

Biological activity of ligand 4e. XTT assay was carried out to evaluate the cytotoxicity of these compounds against human carcinoma cell lines HeLa and A549 as well as in normal human kidney epithelial cell line (NKE). Compound **4e** and **4g** showed significant cytotoxicity towards cancer cell lines (IC_{50} values of 2-6 μM) whereas compound **4h** exhibited weak cytotoxicity with low IC_{50} values (**Table 3**). Interestingly, these three lead compounds displayed negligible cytotoxicity for the human normal cell line.

Table 3. Effect of compounds on the cell viability after 24 h exposure in HeLa, A549 and NKE cell line.

Compounds	IC_{50} (μM)		
	HeLa	A549	NKE
4e	2.5	6.4	> 50
4g	2.0	4.3	> 50
4h	11.5	> 25	> 50

We further carried out dual luciferase reporter assay[52] to study their ability to inhibit oncogenic transcription by interacting with the G-quadruplex (**Figure 6a**). We used plasmid constructs containing wild-type *c-MYC* G-rich promoter sequence[53] (WT *c-MYC* Luc) as well as mutant (G-to-A) *c-MYC* promoter sequence (Mut *c-MYC* Luc) upstream of the firefly coding gene (**Figure 6b**). A control plasmid, pRL-TK (Renilla luciferase, linked to the non G-rich thymidine kinase promoter) was co-transfected with *MYC* Luc constructs as a loading control. HeLa cells were treated with each ligand at concentrations of 1 and 1.5 μM for 36 h after co-transfection. Ligand **4e** reduced the *c-MYC* promoter-linked expression by 31 % and 45 % at 1 and 1.5 μM concentrations (**Figure 6c**).

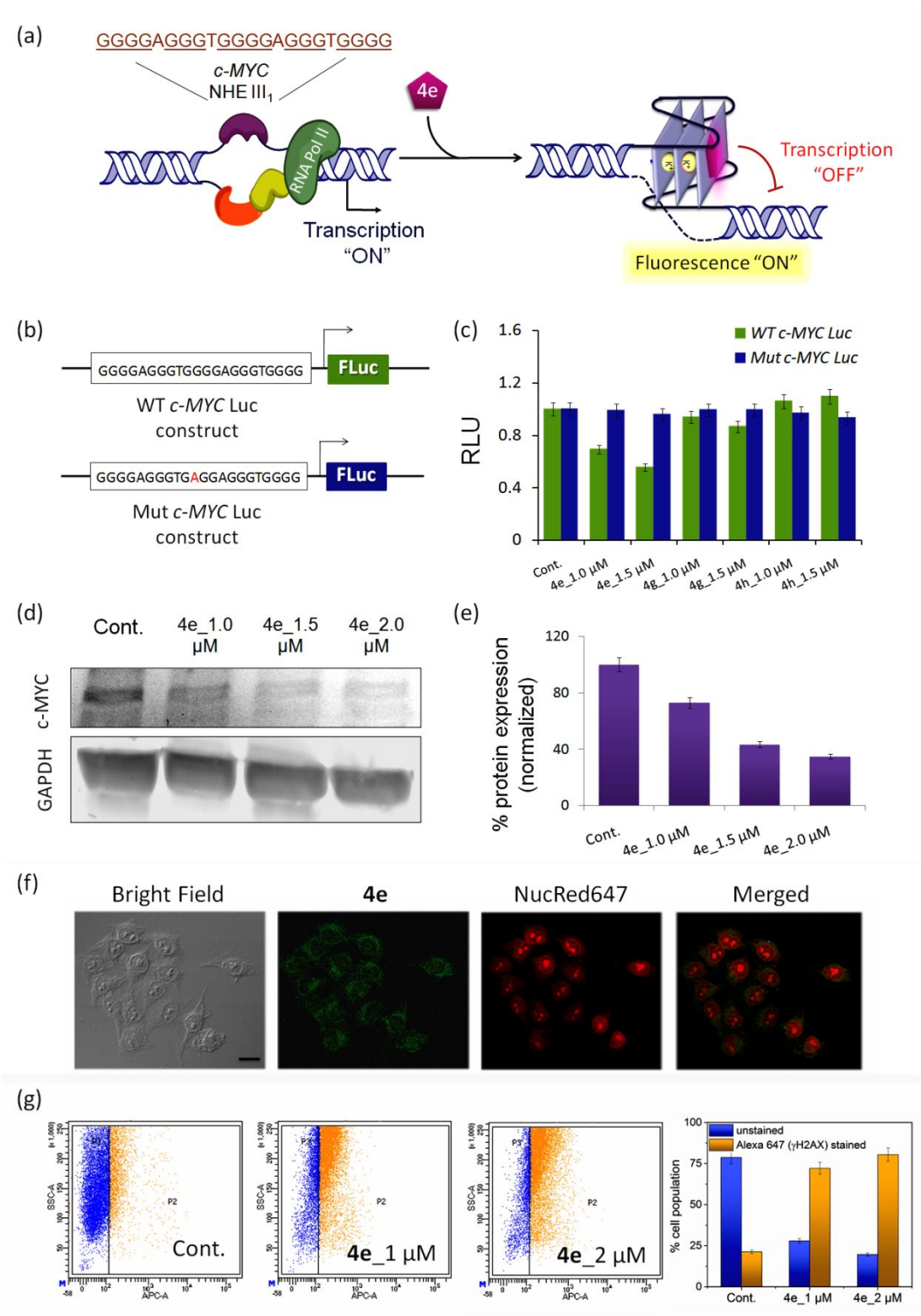

Figure 6. (a) Schematic representation of ligand-mediated downregulation of *c-MYC* gene. (b) Firefly luciferase constructs containing either the WT or mutant *c-MYC* promoter G-

rich sequence. (c) Histogram demonstrating effect of compounds on the *c-MYC* promoter activity, determined by dual luciferase reporter assay. (d) Western Blot bands of *c-MYC* and GAPDH proteins after 24 h treatment with ligand 4e at three different concentrations (1.0 μM, 1.5 μM and 2.0 μM). (e) Bar diagram showing dose-dependent downregulation of *c-MYC* protein by 4e. (f) Confocal imaging of cells treated with 0.5 μM 4e. Nucleus staining dye is NucRed647 and scale bar is 20 μm. (g) Ligand 4e induced DNA damage response in Hela cells as indicated by the increase of Alexa Fluor 647-tagged anti-γ-H2AX stained cell population in Flow cytometry.

However, the transcriptional activity of mutant plasmid construct was not inhibited with increasing concentrations of **4e**. Ligand **4g** exhibited less pronounced transcriptional inhibition (14 % at 1.5 μM) whereas **4h** could not inhibit promoter activity in HeLa cells. The Western Blot analysis confirmed that the major lead compound **4e** could inhibit the MYC expression in HeLa cells in a dose-dependent manner (**Figure 6d-e**). Ligand **4e** repressed the MYC protein expression by 27 % at 1.0 μM, 57 % at 1.5 μM and by 65 % at 2.0 μM concentrations without affecting the expression of the house keeping gene, GAPDH. These results establish that **4e** could downregulate *c-MYC* expression at both transcriptional and translational level by directly targeting its promoter quadruplex.[54-58] Further investigations revealed that the ligand **4e** localizes into the cell as well as within the cell nuclei (**Figure 6f**). To investigate whether ligand **4e** could induce DNA-damage response in cancer cells, flow cytometric assays were carried out with Alexa Fluor 647-tagged anti-γ-H2AX. As shown in Figure 6g, a significant increase in the γ-H2AX foci (a significant marker for DNA damage response) was observed after treatment with **4e** for 24 h at 1 μM and 2 μM concentration. This indicates that ligand **4e** triggers DNA damage

response in cancer cells. Molecular docking studies further revealed that carbazole core of **4e** stacks on the terminal G-quartet plane of G_4-DNA (PDB ID: 1XAV)[59] by π -π interaction and the aromatic cationic side chain interacts with DNA phosphate backbone via electrostatic interactions (**Figure S19a, S.I.**). Interestingly, imine **3e** shows more preferred stacking interactions on G-quartet by mostly exhibiting similar binding mode with G_4-DNA (**Figure S19b, S.I.**). Collectively, these observations gave an understandable explanation regarding the selectivity of **4e** for G_4-DNA compared to other possible amine products.

Conclusions

In conclusion, we have demonstrated that a quadruplex nanotemplate can dynamically select and amplify selective ligands for the quadruplex target from a pool of simple aldehyde and amine building blocks. The present method allows efficient isolation and identification of selective ligands for the quadruplex target as well as the recovery and reuse of DNA nanotemplate. The lead ligand shows significant quadruplex-vs.-duplex selectivity and inhibits gene expression by targeting its promoter quadruplex. The technique highlights quadruplex selective ligands can be developed by using simple and straight-forward synthetic methods in comparison to the previously reported ligands, often associated with synthetic complexity and time-consuming purification and screening processes. In comparison to kinetically controlled TGS approach, where the target selects and promotes irreversible bond formation between the most potent reactive fragments to form the target selective products,[33] the thermodynamically controlled DCC method uses reversible bond formation to generate all possible products and the system evolves and self-corrects in the presence of a target to amplify the best binder at the expense of other products. Together, these results illustrate that nanotemplate guided DCC

method could be potentially useful for the rapid generation of specific ligands for biomacromolecular targets.

EXPERIMENTAL SECTION

General information: All solvents and reagents were purified by standard techniques or used as supplied from commercial sources (Sigma-Aldrich Corporation® unless stated otherwise). All reactions were generally carried out under inert atmosphere unless otherwise noted. TLC was performed on Merck Kieselgel 60 F254 plates, and spots were visualized under UV light. Products were purified by flash chromatography on silica gel (100-200 mesh, Merck). ^{1}H and ^{13}C NMR spectra were recorded on either Bruker ADVANCE 500 (500 MHz and 125 MHz), or JEOL 400 (400 MHz and 100 MHz) instruments using deuterated solvents as detailed and at ambient probe temperature (300 K). Chemical shifts are reported in parts per million (ppm) and are referred to the residual solvent peak. The following notations are used: singlet (s); doublet (d); triplet (t); quartet (q); multiplet (m); broad (br). Coupling constants are quoted in Hertz and are denoted as *J*. Mass spectra were recorded on a Micromass® Q-Tof (ESI) spectrometer with 50% methanol solution. The purity of the synthesized aldehyde (**1**) and the final synthesized compounds (**4a-j**) were confirmed to be higher than 95% by performing HPLC with a dual pump Shimadzu LC-20 AD system equipped with an 5.0 μm ODS2 reverse phase column (4.6 × 250 mm) using 300 nm detection wavelength.

Synthesis of AuMNp. An aqueous solution of $HAuCl_4$ (5 mL, 2.0 mg/mL) was mixed into 20 mL of deionized water and boiled for 5 min. Then, 1 mL Fe_3O_4 nanoparticle solution (synthesized by reported procedure)[33] was added into the reaction mixture followed by the addition of sodium citrate (1 mL, 80 mmol). The color of the solution gradually changed from

brown to burgundy. The reaction mixture was refluxed under stirring for 5 min. After cooling, the solution was sonicated for 10-15 min, and then gold-coated magnetic nanoparticles (AuMNp) were collected using a magnet, washed 3 times and re-dispersed in pure water. Carbazole aldehyde **1** was prepared from commercially available carbazole **S1** (Figure S1).

Synthesis of DNA coated AuMNp (G_4-AuMNp and *ds*DNA-AuMNp). All buffers and solutions were degassed in order to avoid oxidative dimerization into disulfide dimers. Thiolated DNA functionalized nanoparticles were synthesized by derivatizing 100 μL of an aqueous AuMNp nanoparticle solution with 100 μL 5′-thiol capped DNA solution (oligonucleotide concentration is 100 μM in 20 mM MOPS buffer, pH 6.5, 100 mM KCl). Thiolated DNA sequences were pre-annealed in 20 mM MOPS buffer (pH 6.5, 100 mM KCl) by heating at 95 °C for 5 min followed by gradual cooling to room temperature at a controlled rate of 0.1 °C/min and then kept at 4°C for overnight.

After standing for 16 h with AuMNps, nanoparticles were separated using magnet and washed with 20 mM MOPS buffer containing 100 mM KCl (pH 6.5). The volume of the nanoparticle solution was made up to 100 μL with the buffer. The HPLC purified thiol capped DNAs were supplied by SIGMA Aldrich. The sequences of the DNAs are as follows;

G_4-DNA: 5'- [ThiC6] $TG_4AG_3TG_4AG_3TG_4A_2G_2TG_4A$ -3'

*ds*DNA: 5'- [ThiC6] $CA_5T_5GCA_5T_5G$ -3'

Reversible exchange of imines. In a 2 mL eppendorf, aldehyde **1** (20 μL, 10 mM) was taken in 1 mL of MOPS buffer (20 mM, 100 mM KCl, pH 6.5) followed by the addition of amine **2e** (100 μL 10 mM). The mixture was stirred at rt for 12 h. An aliquot of the resulting mixture was

analyzed by ESI mass spectrometry. Then the amine **2d** was added in excess (100 μL 10 mM) to the reaction mixture and the reaction was continued for another 12 h. The final reaction mixture was also analyzed by ESI-MS.

Procedure for G_4-AuMNp templated imine exchange. In a 2 mL eppendorf, 40 μL G_4-AuMNp template (G_4-nanotemplate, ~ 20 μM G_4-DNA) was taken in 500 μL of MOPS buffer (20 mM, 100 mM KCl, pH 6.5). Aldehyde **1** (5 μM) was then added to the mixture, followed by the addition of 25 μM of each amine **2a-j**. The resulting mixture was stirred at rt for 18 h. Then, $NaBH_3CN$ (10 mg) was added to the DCL for the reduction of imines and the resulting mixture was stirred for another 6 h. Subsequently, G_4-AuMNp template was separated from the reaction mixture using a magnet and washed twice with MOPS buffer to remove the unbound amines. Afterwards, the nanoparticles were dispersed in MOPS buffer (50 μL) and the dispersion was then heated for 5 min at 65 °C and the DNA-linked nanotemplate (G_4-AuMNps) was separated instantly. The supernatant containing the amine lead compounds were identified by HPLC and ESI-MS spectroscopy.

Templated imine exchange using *ds*DNA-AuMNp. In a 2 mL eppendorf, 40 μL dsDNA nanotemplate (dsDNA-AuMNp) was added to 0.5 mL of 20 mM MOPS buffer (100 mM KCl, pH 6.5). Aldehyde **1** (5 μM) was then added to the mixture, followed by the addition of 25 μM of each amine **2a-j** building blocks. The resulting mixture was stirred at rt for 18 h. Then $NaBH_3CN$ (10 mg) was added to the DCL and the mixture stirred for another 6 h. After reduction, the lead compounds for dsDNA was identified by following the above-mentioned separation technique.

General procedure for the synthesis of reduced imines (4a-j). Carbazole aldehyde **1** (50 mg, 0.13 mmol) was dissolved in EtOH (4 mL) in the presence of molecular sieves. The desired amine **2 a-j** (0.13 mmol) was added separately and the mixture was stirred for 24 h at room temperature (Figure S11). The resulting reaction mixture comprising imines was dried under vacuum. Then MeOH (5 mL) and $NaBH_3CN$ (20 mg) was added to the solid mass and stirred for another 6 h at room temperature. The mixture was concentrated under vacuum and was purified by flash column chromatography (from CH_2Cl_2 (100%) to CH_2Cl_2/MeOH (10:1) to CH_2Cl_2/MeOH/NH_4OH (10:1:0.5) to give the corresponding amines.

4-(((9-(3-(dimethylamino)propyl)-6-(4-methoxyphenyl)-9H-carbazol-3-yl)methyl)amino)phenol (Amine 4a). Following the **GP**, the reaction of aldehyde **1** with amine **2a** (35.3 mg) afforded **4a** (61 mg, 65 %) as a black viscous liquid. ^{1}H NMR (400 MHz, $CDCl_3$): δ 8.51 (s, 1H), 8.19 (s, 1H), 8.04 (m, 1H), 7.91 (m, 2H), 7.89 (m, 2H), 7.62 (m, 2H), 7.45 (m, 3H), 6.93 (m, 2H), 4.31 (t, *J* = 6.2 Hz, 2H), 3.78 (s, 3H), 3.77 (s, 2H), 2.16 (t, *J* = 7.0 Hz, 2H), 2.13 (s, 6H), 1.92 (m, 2H);^{13}C NMR (100 MHz, $CDCl_3$): δ 157.9, 148.2, 144.5, 141.5, 135.2, 129.8, 129.3, 128.8, 128.6, 128.1, 127.7, 127.4, 127.1, 126.9, 124.1, 123.3, 123.2, 120.9, 109.7, 109.4, 56.5, 55.0, 47.1, 45.5, 41.1, 27.0; HRMS (ESI) Calcd for $C_{36}H_{45}N_4O_2$ $[M+H]^+$ 480.2572, Found 480.2575.

N-((9-(3-(dimethylamino)propyl)-6-(4-methoxyphenyl)-9H-carbazol-3-yl)methyl)-4-nitroaniline (Amine 4b). Following the **GP**, the reaction of aldehyde **1** with amine **2b** (25.3 mg) afforded **4b** (51 mg, 69 %) as a brown viscous liquid. ^{1}H NMR (400 MHz, $CDCl_3$): δ 8.60 (s, 1H), 8.28 (s, 1H), 8.12 (m, 1H), 7.99 (m, 2H), 7.69 (m, 2H), 7.63 (m, 2H), 7.52 (m, 3H), 7.02 (m, 2H), 4.40 (t, *J* = 6.2 Hz, 2H), 3.87 (s, 3H), 3.85 (s, 2H), 2.24 (t, *J* = 7.2 Hz, 2H), 2.22 (s, 6H), 2.01 (m, 2H);^{13}C NMR (100 MHz, $CDCl_3$): δ 158.4, 148.5, 144.5, 141.5, 135.2, 129.8, 129.5, 128.8,

128.6, 128.1, 127.7, 127.5, 127.4, 126.9, 124.1, 123.3, 123.2, 120.9, 109.7, 109.4, 56.4, 55.2, 48.2, 45.5, 41.1, 27.0; HRMS (ESI) Calcd for $C_{36}H_{45}N_4O_2$ $[M+H]^+$ 509.2474, Found 509.2462.

4-bromo-N-((9-(3-(dimethylamino)propyl)-6-(4-methoxyphenyl)-9H-carbazol-3-yl)methyl)-2-methylaniline (Amine 4c). Following the **GP**, the reaction of aldehyde **1** with amine **2c** (30 mg) afforded **4c** (61 mg, 79 %) as a brown viscous liquid. ^{1}H NMR (400 MHz, $CDCl_3$): δ 8.54 (s, 1H), 8.29 (s, 1H), 7.64 (m, 1H), 7.62 (m, 1H), 7.51 (m, 1H), 7.47 (m, 2H), 7.32 (m, 3H), 7.02 (m, 2H), 6.91 (m, 1H), 4.42 (t, *J* = 6.1 Hz, 2H), 3.88 (s, 2H), 3.81 (s, 3H), 3.73 (s, 3H), 2.29 (t, *J* = 6.8 Hz, 2H), 2.24 (s, 6H), 2.05 (m, 2H);^{13}C NMR (100 MHz, $CDCl_3$): δ 158.1, 144.5, 141.5, 135.2, 129.7, 129.1, 128.8, 128.4, 128.1, 127.6, 127.4, 127.3, 127.0, 126.9, 124.1, 123.2, 120.8, 120.5, 111.8, 110.2, 109.7, 109.3, 56.5, 54.9, 51.7, 45.5, 41.3, 26.9, 19.7; HRMS (ESI) Calcd for $C_{36}H_{45}N_4O_2$ $[M+H]^+$ 556.1885, Found 556.1882.

4-(3-(dimethylamino)prop-1-yn-1-yl)-N-((9-(3-(dimethylamino)propyl)-6-(4-methoxyphenyl)-9H-carbazol-3-yl)methyl)aniline (Amine 4d). Following the **GP**, the reaction of aldehyde **1** with amine **2d** (35.3 mg) afforded **4d** (51 mg, 69 %) as a brown viscous liquid. ^{1}H NMR (400 MHz, DMSO-d_6): δ 8.38 (s, 1H), 8.17 (s, 1H), 7.70 (m, 4H), 7.64 (m, 2H), 7.57 (m, 2H), 7.55 (m, 2H), 7.03 (m, 2H), 4.66 (s, 2H), 4.42 (t, *J* = 6.2 Hz, 2H), 3.80 (s, 3H), 3.16 (s, 3H), 2.32 (t, *J* = 7.0 Hz, 2H), 2.20 (s, 12H), 1.93 (m, 2H);^{13}C NMR (100 MHz, DMSO-d_6): δ 158.3, 150.3, 139.8, 139.6, 133.7, 133.2, 130.9, 127.8, 125.5, 124.4, 122.8, 122.1, 118.8, 117.7, 116.2, 115.6, 114.4, 113.3, 109.7, 109.0, 83.7, 82.3, 63.6, 62.7, 55.8, 55.3, 52.2, 48.7, 44.7, 26.1; HRMS (ESI) Calcd for $C_{36}H_{45}N_4O_2$ $[M+H]^+$ 545.3202, Found 545.3213.

4-(3-(dimethylamino)propoxy)-N-((9-(3-(dimethylamino)propyl)-6-(4-methoxyphenyl)-9H-carbazol-3-yl)methyl)aniline (Amine 4e). Following the **GP**, the reaction of aldehyde **1** with amine **2e** (25.3 mg) afforded **4e** (51 mg, 69 %) as a brown viscous liquid. ^{1}H NMR (500 MHz, DMSO-d_6): δ 8.34 (s, 1H), 8.22 (s, 1H), 7.69-7.67 (m, 3H), 7.60 (d, *J* = 8.8 Hz, 1H), 7.53 (d, *J* = 8.2 Hz, 1H), 7.48 (d, *J* = 6.3 Hz, 1H), 7.03-7.01 (m, 2H), 6.67-6.58 (m, 4H), 4.39-4.34 (m, 6H), 3.78 (3H, s), 3.37 (t, *J* = 7.1 Hz, 2H), 2.86 (t, *J* = 5.6 Hz, 2H), 2.23 (s, 6H), 2.18 (s, 6H), 1.91 (m, 2H), 1.82 (m, 2H);^{13}C NMR (125 MHz, DMSO-d_6): δ 158.2, 149.9, 143.3, 142.4, 139.6, 139.5, 133.6, 130.9, 127.6, 125.7, 124.3, 122.6, 122.2, 119.2, 117.6, 115.4, 114.9, 114.3, 113.4, 109.5, 109.1, 66.1, 55.7, 55.3, 55.1, 45.4, 44.6, 44.3, 26.3, 26.0; HRMS (ESI) Calcd for $C_{36}H_{45}N_4O_2$ $[M+H]^+$ 565.35358, Found 565.3535.

N-((9-(3-(dimethylamino)propyl)-6-(4-methoxyphenyl)-9H-carbazol-3-yl)methyl)thiazol-2-amine (Amine 4f). Following the **GP**, the reaction of aldehyde **1** with amine **2f** (32 mg) afforded **4f** (58 mg, 65 %) as a brown viscous liquid. ^{1}H NMR (400 MHz, DMSO-d_6): δ 8.38 (s, 1H), 8.21 (s, 1H), 8.16 (m, 1H), 7.71 (m, 3H), 7.69 (m, 1H), 7.67 (m, 1H), 7.63 (m, 2H), 7.03 (m, 2H), 4.65 (s, 2H), 4.42 (t, *J* = 6.3 Hz, 2H), 3.81 (s, 3H), 2.30 (t, *J* = 6.9 Hz, 2H), 2.19 (s, 6H), 1.94 (m, 2H);^{13}C NMR (100 MHz, DMSO-d_6): δ 169.1, 158.2, 139.7, 139.4, 138.6, 133.6, 133.1, 130.9, 129.6, 127.6, 125.3, 124.2, 122.7, 121.9, 118.7, 117.6, 114.3, 109.5, 106.1, 63.5, 55.7, 55.1, 45.5, 44.5, 25.9; HRMS (ESI) Calcd for $C_{36}H_{45}N_4O_2$ $[M+H]^+$ 471.2140, Found 471.2141.

N-((9-(3-(dimethylamino)propyl)-6-(4-methoxyphenyl)-9H-carbazol-3-yl)methyl)butan-1-amine (Amine 4g). Following the **GP**, the reaction of aldehyde **1** with amine **2g** (9.5 mg) afforded **4g** (46 mg, 69%) as a brown viscous liquid. ^{1}H NMR (500 MHz, DMSO-d_6): δ 8.35 (s,

1H), 8.22 (s, 1H), 7.69 (d, *J* = 7.4 Hz, 3H), 7.61 (d, *J* = 8.3 Hz, 1H), 7.55 (d, *J* = 8.4 Hz, 1H), 7.49 (d, *J* = 8.5 Hz, 1H), 7.04 (d, *J* = 8.3 Hz, 2H), 4.40 (t, *J* = 6.1 Hz, 2H), 3.96 (3H, s), 3.80 (s, 2H), 2.64 (t, *J* = 7.1 Hz, 2H), 2.18 (t, *J* = 6.5 Hz, 2H), 2.12 (s, 6H), 1.90 (m, 2H), 1.50 (m, 2H), 1.32 (m, 2H), 1.23 (t, *J* = 7.1 Hz, 2H), 0.86 (t, *J* = 7.3 Hz, 3H); ^{13}C NMR (125 MHz, DMSO-d_6): δ 158.2, 139.9, 139.5, 133.6, 130.9, 127.7, 126.7, 124.4, 122.6, 122.1, 120.6, 117.6, 114.3, 109.6, 109.0, 56.0, 55.1, 52.7, 52.0, 47.7, 45.1, 30.5, 26.5, 19.8, 13.9; HRMS (ESI) Calcd for $C_{29}H_{38}N_3O$ $[M+H]^+$ 444.3005, Found 444.3008.

N-((9-(3-(dimethylamino)propyl)-6-(4-methoxyphenyl)-9H-carbazol-3-yl)methyl)prop-2-yn-1-amine (Amine 4h). Following the **GP**, the reaction of aldehyde **1** with amine **2h** (7.2 mg) afforded **4h** (33 mg, 59 %) as a yellow liquid . ^{1}H NMR (500 MHz, $CDCl_3$): δ 8.25 (s, 1H), 8.11 (s, 1H), 7.65 (m, 3H), 7.45 (m, 3H), 7.02 (d, *J* = 8.5 Hz, 2H), 4.39 (t, *J* = 6.8 Hz, 2H), 4.08 (s, 2H), 3.88 (s, 3H), 3.50 (d, *J* = 2.0 Hz, 1H), 2.31 (t, *J* = 7.1 Hz, 2H), 2.24 (s, 6H), 2.04 (m, 2H), 1.80 (s, 1H); ^{13}C NMR (100 MHz, $CDCl_3$): δ 158.6, 140.4, 140.0, 134.8, 132.0, 129.9, 128.2, 126.6, 124.9, 123.2, 123.1, 120.3, 118.4, 114.2, 109.0, 108.8, 82.3, 71.5, 56.6, 55.4, 52.7, 45.4, 40.9, 37.3, 29.7, 27.0; HRMS (ESI) Calcd for $C_{28}H_{32}N_3O$ $[M+H]^+$ 426.2545, Found 426.2542.

N1-((9-(3-(dimethylamino)propyl)-6-(4-methoxyphenyl)-9H-carbazol-3-yl)methyl)-N3,N3-dimethylpropane-1,3-diamine (Amine 4i). Following the **GP**, the reaction of aldehyde **1** with amine **2i** (25 mg) afforded **4i** (48 mg, 79 %) as a brown viscous liquid. ^{1}H NMR (400 MHz, $CDCl_3$): δ 8.15 (s, 1H), 7.91 (s, 1H), 7.54 (m, 2H), 7.35 (m, 2H), 7.17 (m, 2H), 7.10 (m, 2H), 4.30 (t, *J* = 6.1 Hz, 2H), 3.79 (s, 3H), 3.73 (s, 2H), 2.55 (t, *J* = 6.0 Hz, 2H), 2.36 (t, *J* = 7.1 Hz, 2H), 2.21 (t, *J* = 6.1 Hz, 2H) 2.20 (t, *J* = 5.9 Hz, 2H), 2.14 (s, 12H), 1.95 (m, 2H);^{13}C NMR (100

MHz, $CDCl_3$): δ 158.3, 148.4, 144.2, 140.6, 135.1, 132.4, 129.7, 129.1, 127.6, 126.7, 125.6, 124.4, 121.8, 120.5, 111.7, 109.6, 65.1, 57.0, 56.2, 55.1, 46.3, 45.5, 41.0, 29.8, 26.9; HRMS (ESI) Calcd for $C_{36}H_{45}N_4O_2$ $[M+H]^+$ 473.3235, Found 473.3233.

N-((9-(3-(dimethylamino)propyl)-6-(4-methoxyphenyl)-9H-carbazol-3-yl)methyl)cyclopropanamine (Amine 4j). Following the **GP**, the reaction of aldehyde **1** with amine **2j** (25.8 mg) afforded **4j** (50 mg, 69 %) as a yellow viscous liquid. ^1H NMR (400 MHz, $CDCl_3$): δ 8.25 (s, 1H), 8.08 (s, 1H), 7.64 (m, 2H), 7.43 (m, 4H), 7.01 (m, 2H), 4.38 (t, J = 6.0 Hz, 2H), 4.04 (s, 2H), 3.87 (s, 3H), 2.32 (t, J = 6.0 Hz, 2H), 2.24 (s, 6H), 2.23 (m, 1H), 2.04 (m, 2H), 0.43 (m, 4H);^{13}C NMR (100 MHz, $CDCl_3$): δ 158.8, 140.4, 140.2, 134.9, 132.2, 130.8, 128.4, 126.8, 125.1, 123.5, 123.2, 120.3, 118.5, 114.4, 109.1, 108.9, 56.8, 55.5, 54.2, 46.1, 45.5, 30.2, 27.0, 9.3; HRMS (ESI) Calcd for $C_{36}H_{45}N_4O_2$ $[M+H]^+$ 428.2657, Found 428.2653.

FRET-based DNA melting assay. FRET melting assay was carried out on a real-time PCR apparatus (Roche LightCycler 480 II) using dual labelled DNA sequences. The DNA sequences labelled with 6-FAM (donor fluorophore) at 5'-end and TAMRA (acceptor fluorophore) at 3'-end were purchased from Eurofins Genomics. The fluorescently labelled oligonucleotides (G_4-DNA and dsDNA) were annealed in 60 mM potassium cacodylate buffer (pH 7.4) at a concentration of 400 nM by heating at 95 °C for 5 min followed by gradual cooling to room temperature at a controlled rate of 0.1 °C/min. Fluorescence melting curves were recorded using a total reaction volume of 100 μL, with 200 nM labelled oligonucleotide in Tris-KCl buffer (pH 7.4) in the absence and/or presence of 1 μM of each amine product (**4a**-**4j**). Measurements were done with excitation at 480 nm and detection at 530 nm. Fluorescence readings were taken with

a ramp rate of 0.01 °C with 30 acquisitions per °C over the range 37−95 °C. Sequences used in the FRET studies are as follows;

G_4-DNA: 5'-FAM -$TG_4AG_3TG_4AG_3TG_4A_2G_2$ - TAMRA-3'

*ds*DNA: 5'- FAM-$CA_5T_5GCA_5T_5G$ - TAMRA-3'

Fluorimetric titration. Fluorescence emission spectra were recorded on incremental addition of DNA into the 0.25 μM ligand solution. The fluorescence spectra were recorded on a Horiba Jobin Yvon Fluoromax 3 instrument at 25 °C in a thermo-stated cell holder using quartz cuvette with a 1 cm path-length. The spectra were taken using filtered and degassed buffer (100 mM Tris.KCl, pH 7.4) solution. DNA sequences used in the biophysical experiments:

G_4-DNA: 5'-$TG_4AG_3TG_4AG_3TG_4A_2G_2$ -3'

*ds*DNA: 5'- $CA_5T_5GCA_5T_5G$ -3'

The binding constants were calculated using the following Hill 1 equation (1) with Origin Pro 8.0:

$$F = F_0 + \frac{(F_{max} - F_0)[DNA]}{K_d + [DNA]} \quad \text{(Equation 1)}$$

where F is the fluorescence intensity, F_{max} is the maximum fluorescence intensity, F_0 is the fluorescence intensity in the absence of DNA and K_d is the apparent dissociation constant.

Fluorescent intercalator displacement (FID) assay. Pre-folded DNA target (0.25 μM) was mixed with thiazole orange (0.50 μM) in Tris–KCl buffer (100 mM, pH 7.4) in a total volume of 0.5 mL and incubated for 30 min at rt. Fluorescence spectrum was recorded after addition of each compound followed by a 3 min equilibration period. The percentage of TO displacement

was calculated from the fluorescence area (F_A, 510–750 nm; excitation, 501 nm) of the spectra using following equation;

% of TO displacement = 100 – [FA × 100/ FA_0]

FA_0 is the fluorescence area from TO bound to the DNA in absence of any ligand. The DC_{50} values were calculated from the plot of percentage of TO displacement vs the concentration of the ligands.

Cell Culture Conditions. Human cervical cancer cell line HeLa, human small lung carcinoma cell line A549, and human normal kidney epithelial cell line NKE were maintained at 37 °C with 5% CO_2. HeLa cells were grown in DMEM (Himedia) and A549 cells are grown in Ham's F12K (Himedia). Normal human cell line was maintained in Glutamine supplemented RPMI 1640 (GIBCO) media. The media were supplemented with 10% FBS (GIBCO) and 1% anti-anti (GIBCO).

XTT cell viability assay. XTT (2,3-bis(2-methoxy-4-nitro-5-sulfophenyl)-5-[(phenylamino)carbonyl]-2*H*-tetrazolium hydroxide) assay was performed to determine the cytotoxicity of the compounds in cells. Viability experiments were performed in triplicate on 96-well plates at designated doses. Cells were grown at a density of 10^4-10^5 cells/well in 100 µL of culture medium and treated with increasing concentrations of the compounds (0-50 µM) and incubated for 24 h. The XTT/PMS reagent was prepared by mixing 1 mg of XTT in 1 mL of culture medium followed by the addition of 2.5 µL of 10 mM PMS solution (in PBS). 25 µL of this freshly prepared reagent mixture was then directly added to each well containing 100 µL of culture media and incubated for 2 h at 37 °C. The absorbance of XTT formazan was read at 450

nm on Multiskan FC microplate spectrophotometer (Thermo Scientific). Percentage cell viability was calculated by using the following equation:

$$\% \text{ of cell viability} = \frac{O.D.\ of\ treated\ cells}{O.D.of\ untreated\ control\ cells} \times 100$$

Dual luciferase reporter assay. 0.2 μg of Del4 plasmid construct (Addgene plasmid #16604-Del4) containing the minimal promoter region of *c-MYC* G-quadruplex sequence was transfected into HeLa cells using Lipofectamine 2000 (Invitrogen). 30 ng of Renilla luciferase plasmid construct (pRL-TK) was co-transfected as a transfection control for normalization. Transfection was performed in serum-free DMEM medium and after 8 h media was replaced with complete media and treated with ligands at respective concentrations. After 36 h, cells were harvested, lysed with 1x passive lysis buffer and luciferase activities of cell lysate were measured using a Dual-Luciferase reporter assay kit (Promega). The assay was also performed with mutant *c-MYC* Del4 plasmid construct (0.2 μg) containing a G-to-A point mutation in the *c-MYC* G-rich region.

Western Blot. Cells were collected after 24 h post-treatment of ligand **4e**, washed with ice cold PBS twice, and lysed with cold cell lysis buffer (20 mM Tris, 100 mM NaCl, 1 mM EDTA in 0.5% Triton X-100) for 30 min on ice, and debris was removed by centrifugation at 12000g for 15 min. Aliquots of the supernatants were used for protein determination by Folin-Lowry method. Equal amounts of protein (70 μg) were subjected to 12 % SDS PAGE, and after gel electrophoresis, the proteins were electrophoretically transferred onto nitrocellulose membranes. Then, membranes were blocked with 4 % BSA for 2 h and then incubated overnight at 4 °C with different primary antibodies. The membranes were washed three times with 1x TBST and then incubated for 2 h with HRP linked respective secondary antibodies. Blots were washed thrice

with 1x TBST and then once with 1x TBS and bands were acquired by the addition of TMB or NBD/BCIP substrate. Relative band intensities were determined by using ImageJ software.

Primary antibodies used:

Anti c-MYC antibody - Rabbit origin (Invitrogen)

Anti GAPDH antibody - Mouse origin (Invitrogen)

Confocal Microscopy of ligand treated cells. The cells were grown on coverslips in six-well plates and treated with 0.5 μM **4e** for overnight. After the incubation, the cells were washed with ice-cold PBS and fixed for 12 min with 1:1 acetone/methanol at –20 °C. The cells were then washed thrice in ice-cold PBS, stained with NucRed 647 Live and kept at room temperature in the dark for 10 min. Images were taken in Olympus confocal laser scanning microscope (model IX81, v 4.1). The raw data was analyzed in Fluoview FV10-ASW v 4.2 software.

Flow cytometry with Alexa fluor 647-tagged anti-γH2AX. Cells were grown in six-well plates and treated with 1 and 2 μM **4e** for overnight. After incubation with the ligand, cells were washed with 1X PBS and collected by trypsinization. The cell pellet was then washed with 1X PBS containing 0.1% FBS. Cells were then fixed with 1 % paraformaldehyde (500 μL) for 30 min at room temperature and then perforated by 0.03 % saponin (freshly prepared in MilliQ water). After 20 min incubation in room temperature with saponin, cells were washed with 1X PBS containing 0.1% FBS. Then the cells were incubated with Alexa fluor 647-tagged anti-γH2AX (50 μL, 1:100 dilution in 1X PBS+0.1% FBS) for 3 h. Next, 300 μL 1X PBS+0.1% FBS mixture was added and cells were then analysed by flow cytometry (BD FACS Aria III).

Binding mode of amine 4e and imine 3e with G_4-DNA. The energy minimized structures of amine **4e** and imine **3e** were obtained with Gaussian 03 using density functional theory (DFT) analysis B3LYP/6-31+G(d) level. Docking studies were performed with the lowest energy conformer of ligands and G_4-DNA (PDB ID: 1XAV)[59] using the Auto-Dock 4.0 program. 30 docking calculations were performed using the Lamarckian genetic algorithm (LGA) with Auto-Dock 4.0 program. The ligand structures were energy minimized using Gaussian 09 (B3LYP/6-31G* level). The coordinates of *c-MYC* (PDB entry: 1XAV) G-quadruplex DNA structure was retrieved and prepared for docking. The grid box was centered on the *c-MYC* G-quadruplex DNA with a grid size enough to encompass the full receptor molecule. Hence, all possible binding modes, intercalation, end stacking, and groove-binding, could be revealed by docking studies. A maximum of 25 million energy evaluations were applied for the experiment. The conformation corresponding to the most cluster members and the lowest binding free energy was selected as the most probable binding conformation. The docked complex structures were imaged using Chimera 1.11.2 software.

ASSOCIATED CONTENT

Supporting Information. The Supporting Information is available free of charge on the ACS Publications website at DOI: 10.1021/acs.jmedchem.XX.

Additional experimental results, ^{1}H and ^{13}C NMR spectra and HPLC chromatograms of the final compounds, reaction schemes, normalized fluorescence responses of ligands, FID curves.

Molecular formula strings

AUTHOR INFORMATION

Corresponding Author

*Phone: +91 33 2473 4971, Ext 1405. Email: ocjd@iacs.res.in

Author Contributions

†These authors contributed equally.

Notes

The authors declare no competing financial interests.

ACKNOWLEDGMENT

JD thanks DST for a SwarnaJayanti fellowship. The authors thank DBT, DST and CSIR-India for research funding. SJ thanks CSIR-INDIA and DP thanks DST, India for research fellowships. The authors thank Mr. Arijit Pal for confocal microscopy, DBT-IPLS unit, University of Calcutta.

REFERENCES

(1) Lehn, J. M. Dynamic combinatorial chemistry and virtual combinatorial libraries. *Chem.-Eur. J.* **1999**, *5*, 2455-2463.

(2) Otto, S.; Furlan, R. L.; Sanders, J. K. M. Recent developments in dynamic combinatorial chemistry. *Curr. Opin. Chem. Biol.* **2002**, *6*, 321-327.

(3) Otto, S.; Furlan, R. L. E.; Sanders, J. K. M. Dynamic combinatorial chemistry. *Drug Discov. Today* **2002**, *7*, 117-125.

(4) Mamidyala, S. K.; Finn, M. G. *In Situ* click chemistry: Probing the binding landscapes of biological molecules. *Chem. Soc. Rev.* **2010**, *39*, 1252-1261.

(5) Corbett, P. T.; Leclaire, J.; Vial, L.; West, K. R.; Wietor, J. L.; Sanders, J. K. M.; Otto S. Dynamic combinatorial chemistry. *Chem. Rev.* **2006**, *106*, 3652-3711.

(6) Hu, X.; Manetsch, R. Kinetic target-guided synthesis. *Chem. Soc. Rev.* **2010**, *39*, 1316-1324.

(7) Cougnon, F. B. L.; Sanders, J. K. M. Evolution of dynamic combinatorial chemistry. *Acc. Chem. Res.* **2011**, *45*, 2211-2221.

(8) Corbett, P. T.; Tong, L. H.; Sanders, J. K. M.; Otto, S. Diastereoselective amplification of an induced-fit receptor from a dynamic combinatorial library. *J. Am. Chem. Soc.* **2005**, *127*, 8902-8903.

(9) Ramström, O.; Lehn, J. M. Drug discovery by dynamic combinatorial libraries**.** *Nat. Rev. Drug Discov.* **2002**, *1*, 26-36.

(10) Hamieh, S.; Ludlow, R. F.; Perraud, O.; West, K. R.; Mattia, E.; Otto S. A synthetic receptor for nicotine from a dynamic combinatorial library. *Org. Lett.* **2012**, *14*, 5404-5407.

(11) Leung, K. C. F.; Arico, F.; Cantrill, S. J.; Stoddart, J. F. Dynamic mechanically interlocked dendrimers: amplification in dendritic dynamic combinatorial libraries. *Macromolecules* **2007**, *40*, 3951-3959.

(12) Ziach, K.; Obrocka-Hrycyna, A.; Jurczak, J. Dynamic combinatorial libraries of 2,5-diformylfuran-derived macrocycles**.** *J. Org. Chem.* **2014**, *79*, 10334-10341.

(13) Gasparini, G.; Molin, M. D.; Prins, L. J. Dynamic approaches towards catalyst discovery. Eur. *J. Org. Chem.* **2010**, 2429−2440.

(14) Li, J.; Nowak, P.; Otto, S. Dynamic combinatorial libraries: from exploring molecular recognition to systems chemistry**.** *J. Am. Chem. Soc.* **2013**, *135*, 9222-9239.

(15) Huc, I.; Lehn, J. M. Virtual combinatorial libraries: dynamic generation of molecular and supramolecular diversity by self-assembly. *Proc. Natl. Acad. Sci. U.S.A.* **1997**, *94*, 2106-2110.

(16) Bunyapaiboonsri, T.; Ramström, O.; Lohmann, S.; Lehn, J. M.; Peng, L.; Goeldner, M. Dynamic deconvolution of a pre-equilibrated dynamic combinatorial library of acetylcholinesterase inhibitors. *ChemBioChem* **2001**, *2*, 438-444.

(17) Shi, B.; Stevenson, R.; Campopiano, D. J.; Greaney, M. F. Discovery of Glutathione S-Transferase inhibitors using dynamic combinatorial chemistry. *J. Am. Chem. Soc.* **2006**, *128*, 8459-8467.

(18) Milanesi, L.; Hunter, C. A.; Sedelinkova, S. E.; Waltho, J. P. Amplification of bifunctional ligands for calmodulin from a dynamic combinatorial library. *Chem.–Eur. J.*, **2006**, *12*, 1081-1087.

(19) Klekota, B.; Hammond, M. H.; Miller, B. L. Generation of novel DNA-binding compounds by selection and amplification from self-assembled combinatorial libraries. *Tetrahedron Lett.* **1997**, *38*, 8639-8642.

(20) Bugaut, A.; Toulmé, J. J.; Rayner, Use of dynamic combinatorial chemistry for the identification of covalently appendend residue that stabilize oligonucleotide complexes. *Angew. Chem. Int. Ed.* **2004**, *43*, 3144-3147.

(21) Bugaut, A.; Bathany, K.; Schmitter, J. M.; Rayner, B. Target-induced selection of ligands from a dynamic combinatorial library of mono- and bi-conjugated oligonucleotides. *Tetrahedron Lett.* **2005**, *46*, 687-690.

(22) Whitney, A. M.; Ladame, S.; Balasubramanian, S. Templated ligand assembly by using g-quadruplex DNA and dynamic covalent chemistry. *Angew. Chem. Int. Ed.* **2004**, *43*, 1143-1146.

(23) Ladame, S.; Whitney, A. M.; Balasubramanian, S. Targeting nucleic acid secondary structures with polyamides using an optimized dynamic combinatorial approach. *Angew. Chem. Int. Ed.* **2005**, *44*, 5736-5739.

(24) Bugaut, A.; Jantos, K.; Wietor, J. L.; Rodriguez, R.; Sanders, J. K.; Balasubramanian, S. Exploring the differential recognition of DNA G-quadruplex targets by small molecules using dynamic combinatorial chemistry. *Angew. Chem. Int. Ed.* **2008**, *47*, 2677-2680.

(25) Karan, C.; Mille, B. L. RNA-selective coordination complexes identified via dynamic combinatorial chemistry. *J. Am. Chem. Soc.* **2001**, *123*, 7455-7456.

(26) Gareiss, P. C; Sobczak, K.; McNaughton, B. R.; Palde, P. B.; Thornton, C. A.; Miller, B. L. Dynamic combinatorial selection of molecules capable of inhibiting the (CUG) repeat RNA−MBNL1 interaction in vitro: discovery of lead compounds targeting myotonic dystrophy (DM1). *J. Am. Chem. Soc*. **2008**, *130*, 16254-16261.

(27) Ofori, L. O.; Hoskins, J.; Nakamori, M.; Thornton, C. A.; Miller, B. L. From dynamic combinatorial 'hit' to lead: *in vitro* and *in vivo* activity of compounds targeting the pathogenic RNAs that cause myotonic dystrophy. *Nucleic Acids Res.* **2012**, *40*, 6380-6390.

(28) McNaughton, B. R.; Miller, B. L. Resin-bound dynamic combinatorial chemistry**.** *Org. Lett.* **2006**, *8*, 1803-1806.

(29) Nowak, P.; Saggiomo, V.; Salehian, F.; Colomb-Delsuc, M.; Han, Y.; Otto, S. Localized template-driven functionalization of nanoparticles by dynamic combinatorial chemistry. *Angew. Chem. Int. Ed.* **2015**, *54*, 4192-4197.

(30) Han, Y.; Nowak, P.; Colomb-Delsuc, M.; Leal, M. P.; Otto, S. Instructable nanoparticles using dynamic combinatorial chemistry. *Langmuir* **2015**, *31*, 12658-12663.

(31) Otto, S.; Furlan, R. L. E.; Sanders, J. K. M. Dynamic combinatorial libraries of macrocyclic disulfides in water. *J. Am. Chem. Soc.* **2000**, *122*, 12063-12064.

(32) Chakravarthi, S.; Jessop, C. E.; Bulleid, N. J. The role of glutathione in disulphide bond formation and endoplasmic-reticulum-generated oxidative stress. *EMBO Rep*. **2006**, *7*, 271-275.

(33) Panda, D.; Saha, P.; Das, T.; Dash, J. Target guided synthesis using dna nano-templates for selectively assembling a G-quadruplex binding *c-MYC* inhibitor. *Nat. Commun.* **2017**, *8*, 16103.

(34) Huppert, J. L.; Balasubramanian, S. Prevalence of quadruplexes in the human genome. *Nucleic Acids Res*. **2005**, *33*, 2908-2916.

(35) Murat, P.; Balasubramanian, S. Existence and consequences of G-quadruplex structures in DNA. *Curr. Opin. Genet. Dev*. **2014**, *25*, 22-29.

(36) Chambers, V. S.; Marsico, G.; Boutell, J. M.; Antonio, M. Di; Smith, G. P.; Balasubramanian, S. High-throughput sequencing of DNA G-quadruplex structures in the human genome. *Nat. Biotechnol*. **2015**, *33*, 877-881.

(37) Neidle, S. Quadruplex nucleic acids as novel therapeutic targets. *J. Med. Chem.* **2016**, *59*, 5987-6011.

(38) Hansel-Hertsch, R.; Antonio, M. Di; Balasubramanian, S. DNA G-quadruplexes in the human genome: detection, functions and therapeutic potential. *Nat. Rev. Mol. Cell. Bio.* **2017**, *18*, 279-284.

(39) Neidle, S. Quadruplex nucleic acids as targets for anticancer therapeutics. *Nat. Rev. Chem*. **2017**, *1*, 0041.

(40) Brockmann, A.; Strittmatter, T.; May, S.; Stemmer,K.; Marx, A.; Brunner, T. Structure–function relationship of thiazolide-induced apoptosis in colorectal tumor cells. *ACS Chem.Biol.* **2010**, *9*, 1520-1527.

(41) Monchaud, D.; Teulade-Fichou, M. P. A hitchhiker's guide to G-quadruplex ligands**.** *Org. Biomol. Chem.* **2008**, *6*, 627-636.

(42) Tian, T.; Chen, Y. Q.; Wang, S. R.; Zhou, X. G-quadruplex: A regulator of gene expression and its chemical targeting. *Chem* **2018**, *4*, 1314-1344.

(43) Tera, M.; Ishizuka, H.; Takagi, M.; Suganuma, M.; Shin-ya, K.; Nagasawa, K. Macrocyclic hexaoxazoles as sequence-and mode-selective G-quadruplex binders. *Angew. Chem. Int. Ed.*, **2008**, *47*, 5557–5560.

(44) Maji, B.; Kumar, K.; Kaulage, M.; Muniyappa, K.; Bhattacharya, S. Design and synthesis of new benzimidazole–carbazole conjugates for the stabilization of human telomeric DNA, telomerase inhibition, and their selective action on cancer cells. *J. Med. Chem.* **2014**, *57*, 6973-6988.

(45) Zhang, X.; Chi, L.; Ji, S.; Wu, Y.; Song, P.; Han, K.; Guo, H.; James, T. D.; Zhao, J. Rational design of d-PeT phenylethynylated-carbazole monoboronic acid fluorescent sensors for the selective detection of α-hydroxyl carboxylic acids and monosaccharides. *J. Am. Chem. Soc.* **2009**, *131*, 17452-17463.

(46) Zhao, L.; Wagner, P.; Elliott, A. B. S.; Griffith, M. J.; Clarke, T. M.; Gordon, K. C.; Mori, S.; Mozer, A. J. Enhanced performance of dye-sensitized solar cells using carbazole-substituted di-chromophoric porphyrin dyes. *J. Mater. Chem. A* **2014,** *2*, 16963-16977.

(47) Wang, C.; Jia, G.; Zhou, J.; Li, Y.; Liu, Y.; Lu, S.; Li, C. Enantioselective Diels–Alder reactions with G-quadruplex DNA-based catalysts. *Angew. Chem. Int. Ed.* **2012**, *51*, 9352-9355.

(48) Siddiqui-Jain, A.; Grand, C. L.; Bearss, D. J.; Hurley, L. H. Direct evidence for a G-quadruplex in a promoter region and its targeting with a small molecule to repress c-MYC transcription. *P. Natl. Acad. Sci. USA* **2002**, *99*, 11593-11598.

(49) Mathad, R. I.; Hatzakis, E.; Dai, J. X.; Yang, D. Z. c-MYC promoter G-quadruplex formed at the 5′-end of NHE III_1 element: insights into biological relevance and parallel-stranded G-quadruplex stability. *Nucleic Acids Res.* **2011**, *39*, 9023-9033.

(50) De Cian, A.; Guittat, L.; Kaiser, M.; Sacca, B.; Amrane, S.; Bourdoncle, A.; Alberti, P.; Teulade-Fichou, M. P.; Lacroix, L.; Mergny, J. L. Fluorescence-based melting assays for studying quadruplex ligands. *Methods* 2007, **42**, 183-195.

(51) Monchaud, D; Allain, C.; Bertrand, H.; Smargiasso, N.; Rosu, F.; Gabelica, V.; De Cian, A.; Mergny, J. L.; Teulade-Fichou, M. R. Ligands playing musical chairs with G-quadruplex DNA: a rapid and simple displacement assay for identifying selective g-Guadruplex binders. *Biochimie* **2008**, *90*, 1207-1223.

(52) Halder, K.; Benzler, M.; Hartig, J. S. Reporter Assays for studying quadruplex nucleic acids. *Methods* **2012**, *57*, 115-121.

(53) He, T. C.; Sparks, A. B.; Rago, C.; Hermeking, H.; Zawel, L.; da Costa, L. T.; Morin, P. J.; Vogelstein, B.; Kinzler, K. W. Identification of c-MYC as a target of the APC pathway. *Science* **1998**, *281*, 1509-1512.

(54) Kumar, Y. P.; Saha, P.; Saha, D.; Bessi, I.; Schwalbe, H.; Chowdhury, S.; Dash, J. Fluorescent dansyl-guanosine conjugates that bind *c-MYC* promoter G-quadruplex and downregulate *c-MYC* Expression. *ChemBioChem* **2016**, *17*, 388-393.

(55) Chauhan, A.; Paul, R.; Debnath, M.; Bessi, I.; Mandal, S.; Schwalbe, H.; Dash, J. Synthesis of fluorescent binaphthyl amines that bind *c-MYC* G-quadruplex DNA and repress *c-MYC* expression. *J. Med. Chem.* **2016**, *59*, 7275-7281.

(56) Felsenstein, K. M.; Saunders, L. B.; Simmons, J. K.; Leon, E.; Calabrese, D. R.; Zhang, S. L.; Michalowski, A.; Gareiss, P.; Mock, B. A.; Schneekloth, J. S. Small molecule microarrays

enable the identification of a selective, quadruplex-binding inhibitor of MYC expression. *ACS Chem. Biol.* **2016**, *11*, 139-148.

(57) Hu, M. H.; Wang, Y. Q.; Yu, Z. Y.; Hu, L. N.; Ou, T. M.; Chen, S. B.; Huang, Z. S.; Tan, J. H. Discovery of a new four-leaf clover-like ligand as a potent *c-MYC* transcription inhibitor specifically targeting the promoter G-quadruplex**.** *J. Med. Chem.* **2018**, *61*, 2447-2459.

(58) Dutta, D.; Debnath, M.; Müller, D.; Paul, R.; Das, T.; Bessi, I.; Schwalbe, H.; Dash, J. Cell penetrating thiazole peptides inhibit c-MYC expression via site-specific targeting of *c-MYC* G-quadruplex. *Nucleic Acids Res.* **2018**, *46,* 5355-5365.

(59) Phan, A.T.; Modi, Y. S.; Patel, D. J. Propeller-type parallel-stranded G-quadruplexes in the human c-myc promoter. *J. Am. Chem. Soc.* **2004**, *126*, 8710-8716.

Table of Contents graphic: